A Dictionary Learning Approach for Noise-Robust Image Reconstruction in Low-Field Magnetic Resonance Imaging

Ahishakiye, Emmanuel; van Gijzen, Martin Bastiaan; Tumwiine, Julius ; Obungoloch, Johnes

Publication date
2020

Document Version
Final published version

Published in
2020 IST-Africa Conference (IST-Africa)

IST-Africa

IST-Africa 2020 Conference Proceedings
Miriam Cunningham and Paul Cunningham (Eds)
IST-Africa Institute and IIMC, 2020
ISBN: 978-1-905824-65-6

A Dictionary Learning Approach for Noise-Robust Image Reconstruction in Low-Field Magnetic Resonance Imaging

Emmanuel AHISHAKIYE[1,2], Martin Bastiaan VAN GIJZEN[3], Julius TUMWIINE[4], Johnes OBUNGOLOCH[1]

[1]*Department of Biomedical Sciences and Engineering, Mbarara University of Science and Technology, Mbarara, 1410, Uganda, Tel: +256787371879, +256775646496*
Email: ahishema@gmail.com, jobungoloch@must.ac.ug
[2]*Department of Computer Science, Kyambogo University, PO Box 1, Kampala, Uganda*
[3] *Delft Institute of Applied Mathematics, Delft University of Technology, The Netherlands, Email: M.B.vanGijzen@tudelft.nl*
[4]*Department of Mathematics, Mbarara University of Science and Technology, P.O. Box 1410, Mbarara, Uganda, Email: jtumwiine@must.ac.ug*

Abstract: ***Objective:*** Image denoising has been considered as a separate procedure from image reconstruction which could otherwise be combined with acquisition and reconstruction. This paper discusses a joint image reconstruction and denoising algorithm in low-field MRI using a dictionary learning approach. ***Method:*** Our proposed algorithm uses a two-level Bregman iterative method for image reconstruction and image denoising procedure using OMP for sparse coding and SimCO for Dictionary Update and Learning. ***Results:*** Experiments were done on a noisy phantom that was obtained from a low field MRI scanner. Results demonstrate that our proposed algorithm performs superior image reconstructions that are almost noise-free. Our proposed method also performed better than the TBMDU algorithm, which performed better than DLMRI, a technique that substantially outperformed other CSMRI based reconstruction methods. However, the TBMDU algorithm is faster than our proposed algorithm due to additional iterations required during the denoising step. ***Conclusion:*** An algorithm that jointly performs reconstruction and denoising is essential in medical imaging modalities where image denoising has been a separate process from the reconstruction. Combining the two could save time and could avoid image details to be lost due to having two separate operations. This formulation is essential in imaging modalities like low-field MRI where the image signal is noisy and therefore performing a joint reconstruction and denoising could help improve the quality of the images obtained.

Keywords: Dictionary learning, Two-level Bregman iterative method, Image Reconstruction, Image denoising, low-field MRI.

1. Introduction

Magnetic Resonance Imaging (MRI) is a safe medical imaging technology that provides a non-invasive way to view the structure of human anatomy [1]. MRI systems are classified according to the strength of the magnetic field they produce (in Tesla): Ultra-High Field > 3T, High Field (1 - 3T), Mid Field (0.5 - 1T), Low Field (0.1- 0.5T) and Ultra-Low Field < 0.1T [2]. However, conventional MRI scanners (high-field) are very expensive to purchase, operate and maintain in developing countries [2]. Due to these limitations, many people in developing countries do not have access to MRI technology [3]: for example, Uganda, with a population of nearly 45 million, has only 4 MRI machines and there are 84 MRI machines in West Africa serving a combined population of more than 350 million [4].

To address the above challenges, teams from Mbarara University of Science and Technology (MUST) in Uganda, Leiden University Medical Centre (LUMC) in the Netherlands, Delft University of Technology (TU Delft) in the Netherlands, and Pennsylvania State University (PSU) in the USA are working on developing affordable, portable and low-field MRI scanners, aiming to diagnose children in developing countries with hydrocephalus [3]. Hydrocephalus is a condition where there is an excessive accumulation of cerebrospinal fluid in the brain leading to distention of the ventricular system of the brain. In hydrocephalic children, the critical issue is to distinguish between brain matter and cerebrospinal fluid (CSF) to be able to make treatment decisions. This distinction does not require very high-resolution images be make and therefore an appropriate low-field MRI system would be able to provide images that make the distinction possible [2]. For the beginning, we are targeting the use of the low-field MRI devices under development for hydrocephalus diagnosis (imaging). It is after the achievement of this objective we plan to scale the devices beyond hydrocephalus.

Our research is part of a larger programme funded by the Dutch organization NWO-WOTRO to stimulate research that addresses the Sustainable Development Goals (SDGs). By developing low-cost MRI scanners, we aim to contribute to SDG 3: “Ensure healthy lives andpromote well-being for all at all ages”. Figure 1.1 shows our low-field MRI prototypes.

Figure 1.1: The low-field MRI prototypes. Left is the PSU-MUST prototype, taken from [2]; and right is the LUMC prototype, taken from [4].

The low-field MRI systems above (PSU-MUST and LUMC prototypes) are characterized by a low signal-to-noise ratio, and this has a very big impact on the quality of the final image [5]. Also, the images generated are very noisy (see Figure 1.2), and it takes a long time to acquire an image (takes more than 16 minutes to scan an object). With the algorithm that is described in this paper we aim to alleviate these drawbacks of low-field MRI. Our project is ongoing and we expect to start clinical trials in the first half of 2021. The LUMC prototype will be shipped in the spring of 2020 for testing at MUST in Uganda.

According to literature, two major attempts have been made to increase the imaging speed for MRI systems; these are hardware and software approaches. The hardware approach uses a multichannel parallel MRI, its limitation being economically expensive and requires considerable time in development. The use of a hardware approach is beyond the scope of this study. The software approach uses compressed sensing, which guarantees accurate reconstruction of good quality diagnostic MR images from fewer signals than those mandated by Nyquist sampling [6] [7]. Compressed sensing techniques like dictionary learning, can help us improve on the signal-to-noise ratio of the generated images as well as noise removal, and also improvement in the imaging speed of the low-

field MRI systems since it is possible to reconstruct a good quality diagnostic image with 20-30% of the k-space data [6]. Figure 1.2 shows some of the images from our low-field MRI prototypes.

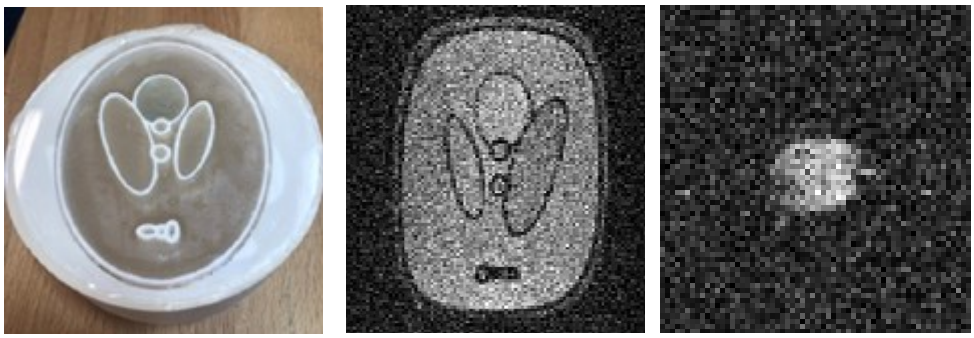

Figure 1.2: Images showing relatively high SNR but also image distortions. (Left) The phantom (Shepp Logan) is 3D printed with dimensions 10x10x3.5 cm^3 and filled with oil. (Middle) The image was acquired using a spin-echo sequence with no slice selection gradient, and a spatial resolution of 1x1x35 mm^3. Eight signal averages were acquired with a total data acquisition time of 16 min. Adapted from [4]. *The image on the right (oval) was obtained with the PSU-MUST prototype, while that in the middle was obtained with the LUMC prototype.*

1.1 Application of Compressed Sensing to low-field MRI

In the natural sciences, inverse problems are often ill-posed, and their solutions are very sensitive to perturbations in the data. An example of such an ill-posed problem is the reconstruction of an image based on low-field Magnetic Resonance Imaging (MRI) [5]. Compressed Sensing (CS) theory [6] have been applied in ill-posed inverse problems including image construction [7], [8], [9], [10], [11], [12], [13], [14] and image denoising [15], [16]. Our interest is to develop a joint image reconstruction and denoising algorithm that can be used in low-field MRI systems. The model for image reconstruction is described by Eq. (1) below:

$$\min_u J(u) = \|\Psi u\|_0 \text{ Subject to } F_p u - f = 0 \qquad (1)$$

where u $\in \mathbb{C}^P$ represents the vector of the 2D complex image to be reconstructed, $f \in \mathbb{C}^m$ represents the k-space measurements, $\Psi \in \mathbb{C}^{T \times p}$ represents the sparsifying transform like wavelet transform, $\|.\|_0$ represents the number of non-zero elements in the vector, $F_p \in \mathbb{C}^{m \times p}$ represents the undersampled Fourier encoding matrix and $J(u)$ is the sparsity promoting regularization criteria subject to data consistency $F_p u - f$ (in the absence of noise). Undersampling occurs whenever the number of k-space measurements is less than the number of unknowns i.e. m < P. In the presence of noise, for example, White Gaussian noise, the Eq. (1) is formulated as in Eq. (2)

$$\min_u J(u) = \|\Psi u\|_0 \text{ subject to } \|F_p u - f\|_2 \leq \sigma \qquad (2)$$

where σ is the standard deviation of the noise added to the measured k-space data.

Compressed Sensing reconstructs the unknown u from the measurements f, or by solving the underdetermined system of linear equations $F_p u = f$ by minimizing the ℓ_0 quasi norm (the number of non-zero elements) of the sparsified image Ψu, where Ψ represents a global sparsifying transform of the image. This ℓ_0 problem in Eq. (1) and (2), sometimes called sparse coding problem because it corresponds to finding a sparse code u for a given vector f using the cookbook F_p, is NP-hard. Greedy algorithms such as Orthogonal Matching Pursuit (OMP) have been used to solve this problem. Alternatively, the problem is solved by replacing the ℓ_0 quasi norm with its convex relaxation, the ℓ_1 quasi norm [8], which can be solved by linear programming in a real case or second-order cone programming in the complex case. Compressed Sensing has been applied to a variety of MR modalities such as static MRI, dynamic MRI, diffusion tensor imaging (DTI), and

perfusion imaging. In this study, we restrict our attention to Compressed Sensing for static MRI, in particular, low-field MRI, and study it in detail.

1.2 Research Objectives and Outline

An efficient joint image reconstruction and denoising method can be of great importance especially in low-field MRI imaging. There are many sources of noise during imaging especially in low-field MRI that renders obtained signals or images noisy. Such noise should be removed before subsequent operations are done like segmentation, classification or before being used by clinicians in their diagnosis tasks. Image denoising has been used as a separate operation from image reconstruction, and therefore doing both operations differently consumes time that could otherwise be saved if the operations are combined in one algorithm. This study is incremental in nature; it seeks to integrate image reconstruction and denoising algorithms. Therefore, the major objective of this study is to develop and implement a noise-robust image reconstruction algorithm suitable for medical imaging devices like in low-field MRI systems that are characterized by noise.

The rest of the paper is organized as follows. In section 2, the methodology is discussed; section 2.1 discusses the Two-Level Bregman Method for Image Reconstruction in MRI; section 2.2 discusses image denoising algorithms, and section 2.3 discusses our proposed algorithm. In section 3, Experiments and results are discussed. Section 4 discusses the comparison of our proposed formulation with other algorithms and Conclusions and Outlook are given in section 5.

2. Methods

2.1 Two-Level Bregman Method for Image Reconstruction in MRI

The Two-Level Bregman image reconstruction algorithm adopted in this paper was initially proposed by [7]. The algorithm consists of a two-level solver employing the Bregman technique. One part is to estimate the recovery image and the other part is to calculate the dictionary and sparse coefficients of image patches. A modified strategy is applied to the sparse coding step of the inner minimization, enabling the efficiency of the proposed algorithm. For more details, readers can refer to Ref. [7].

The following section summarizes the derivation of the Two-Level Bregman image reconstruction algorithm from the original Bregman iterative method.

The Bregman iterative method is used to solve the following problem

$$\min_u J(u) \text{ Subject to } H(u) = 0 \tag{3}$$

where J and H are convex functions. H is also differentiable.

The formulation in Eq. (3) can be transformed by the Bregman method into a series of unconstrained sub-problems as shown in Eq. (4)

$$\begin{cases} u^{k+1} = argmin\ B_j^{s^k}(u, u^k) + H(u) \\ s^{k+1} = s^k - \nabla H(u^{k+1}) \end{cases} \tag{4}$$

where $B_j^s(x,y) = J(x) - J(y) - \langle s, x-y \rangle$. s is a sub-gradient of $J(u)$ at the point y.

A newly updated formulation is obtained by substituting $H(u) = \mu \left\| F_p u - f \right\|_2^2 /2$, $f^k = F_p s^k / \mu$ as shown in Eq. (5).

$$\begin{cases} u^{k+1} = argmin_u\ J(u) + \frac{\mu}{2} \left\| F_p u - f^k \right\|_2^2 \\ f^{k+1} = f^k + f - F_p u^{k+1} \end{cases} \tag{5}$$

where $f^0 = 0$ and $\mu > 0$ is a weighting parameter.

A two-level Bregman iterative method is formulated by substituting the regularization term $J(u) = \sum_i \left(\|\alpha_i\|_1 + \frac{\lambda}{2} \|D\alpha_i - R_i\mu\|_2^2 \right)$ in Eq. (5) and a new formulation (Eq. 6) is obtained.

$$\begin{cases} u^{k+1} = argmin_u \left\{ \min_{D,\Gamma} \sum_i \left(\|\alpha_i\|_1 + \frac{\lambda}{2} \|D\alpha_i - R_i\mu\|_2^2 \right) + \frac{\mu}{2} \|F_p u - f^k\|_2^2 \right\} \\ f^{k+1} = f^k + f - F_p u^{k+1} \end{cases} \quad (6)$$

where $u \in C^N$ represents the image to be reconstructed, $f \in C^K$ represents the undersampled Fourier measurements, C represents the complex field and $R_i\mu$ denotes the i^{th} patch extracted from image u. $F_p \in C^{KxN}$ Represents the partially sampled Fourier encoding matrix that maps u to f such that $F_p u - f$, D = [d_1, d_2,---, d_q] $\in C^{MxQ}$ and Γ = $[\alpha_1, \alpha_2, ---, \alpha_I] \in C^{QxI}$. The parameter λ balances the sparse level of the image patches and the approximation error in the updating dictionary. For many natural or medical images, the value λ can be determined empirically. For more details, readers can refer to Ref. [7].

The frequency interpolation on line 10 in the algorithm is achieved by the following equations (Eq. 8 and 9).

$$S_1 = FF_p^T f^k \quad (7)$$

$$S_2 = \frac{F \sum_i R_i^T (D^{k+1}\alpha_i^{k+1} + z_i^{k+1} - y_i^{k+1}/\beta}{\omega} \quad (8)$$

$$Fu(k_x, k_y) = \begin{cases} S_2(k_x, k_y), (k_x, k_y) \notin \Omega \\ \frac{\mu S_1(k_x, k_y) + \beta S_2(k_x, k_y)}{\mu + \beta} \\ (k_x, k_y) \in \Omega \end{cases}, \quad (9)$$

where $Fu(k_x, k_y)$ represents the updated value at the location (k_x, k_y), Ω stands for the subset of k-space that has been sampled. Equations 8 and 9 are referred to as frequency interpolation step.

In summary, the two-level Bregman iterative method consists of two-level nested loops. The outer loop updates the value of f^k while the inner loop updates the variables *D,* Γand *u.* using algorithm 1, for the outer loop, the value of f^k is progressively updated to obtain the minimum of (1) or (2). The inner loop employs the two-step approach, iteratively attaining sparse representation of the image patches and updating (8) and (9), to minimize the penalty function for the given value of f^k.

There are four parameters involved i.e. μ, ⋋, β and $\mathcal{E}$. The parameters μ and ⋋ are positive parameters for Bregman/AL iteration algorithms. The values of μ and β have little effect on the final reconstruction quality provided they are sufficiently small. Furthermore, it should be noted that the smaller the value of the Bregman parameters are, the more iterations are needed to reach the stop criteria. ⋋ stands for the sparse level of the image patches and can be determined empirically. As to the step size $\mathcal{E}$ for updating the dictionary, it can be set as a small positive number such as 0.01. For more details, readers can refer to Ref. [7].

2.2 Image Denoising

The image denoising algorithm adopted in this paper was initially proposed by [17]. The approach that was used in their study was based on sparse and redundant representations where the proposed algorithm denoises the image while simultaneously training a

dictionary using Simultaneous Codeword Optimization (SimCO) algorithm. For more details, readers can refer to Ref. [17].

Consider the following image denoising formulation in Eq. (10)

$$\{\hat{D}, \hat{\alpha}_{ij}, \hat{X}\} = \arg\min_{\hat{D},\alpha_{ij},X} \lambda \|X-Y\|_2^2 + \sum_{ij} \mu_{ij} \|\alpha_{ij}\|_0 + \sum_{ij} \|D\alpha_{ij} - R_{ij}X\|_2^2 \quad (10)$$

where Y is the measured image, X is the noised version of Y, D is the dictionary, α is the sparse code and $\|\alpha\|_0$ represents non-zero entries in α.

The formulation in Eq. (10) has three unknowns: (1) the dictionary D, (2) the sparse representations α_{ij} and (3) the overall denoised image output X. The formulation in Eq. (10) was solved by using a block-coordinate minimization algorithm that fixes two of the unknowns, and searching for the optimal third. The sparse representation α_{ij} is solved using the orthonormal matching pursuit (OMP) [18] and the dictionary D is updated using the K-SVD algorithm [19]. Then finally the sparse representation α_{ij} and updated dictionary D are fixed to update X. therefore, in summary, the above-proposed image denoising algorithm performs sparse coding of small image patches using OMP, performs dictionary update using KSVD and averaging the resulting image patches as the final step in the algorithm. Experiments performed using the proposed algorithm showed excellent results even when the dictionary was trained in a noisy image. However, the K-SVD algorithm for dictionary learning and updating is slow because it updates dictionary atoms (codewords) individually [20]. The study by [20] proposed an algorithm called Simultaneous Codeword Optimization (SimCO) for Dictionary Update and Learning that overcomes the challenges of KSVD. Instead of updating atoms (codewords) individually, SimCO simultaneously updates all the codewords. Hence, SimCO is faster than K-SVD in dictionary learning and updating operations. For more details, readers can refer to Ref. [20].

2.3 The proposed denoising driven reconstruction algorithm

Our proposed approach is to reconstruct natural and medical images such as the one shown in Fig. (2) using a two-level Bregman iterative method while simultaneously denoising the image during reconstruction. Our proposed algorithm is also robust to noise such as zero-mean white Gaussian noise. The main task here is to reconstruct an image using the Two-Level Bregman Method (TBMDU) [7] followed by denoising [20]. Fig 3 shows the proposed algorithm. Our proposed algorithm consists of two steps: (1) image reconstruction step based on Algorithm 1 and (2) image denoising step based on algorithm2. The image denoising step uses SimCO for dictionary updating and OMP for sparse coding. In our formulation, the output from step 1 (i.e. image reconstruction step) is fed into step 2 (i.e. image denoising step). The results from our experiments show that our proposed methods perform well in both reconstruction and denoising even when the input image had natural noise (noise obtained from the imaging system) and when noise e.g. white mean Gaussian noise was added to the image. The novelty of this work is incremental. During our study, we integrated image reconstruction and denoising. The practical significance of this proposed algorithm is its applications in joint image reconstruction and denoising especially in the low-field and ultralow-field MRI systems. These systems are characterized by low signal to noise ratio and therefore the final images have noise which needs to be removed before the image is used for clinical use.

Algorithm1: Proposed algorithm for image reconstruction and denoising

---

1. Initialization: $\Gamma^0 = 0$, $C^0 = 0$, D^0, $u^0 = F_p^T f, f^0 = f$.
2. ***while*** $\| F_p u^k - f \|_2 > \sigma$ ***do***
3. i = 1
4. ***while*** i ≤ P ***do***
5. ***while*** stop criterion not satisfied ***do***
6. $Y^{m+1} = \frac{\lambda\beta}{\lambda+\beta}(-D^{i,m} + Ru^{k,i} + C^i/\beta)$
7. $\Gamma^{i,m+1} = shrink\left(\Gamma^{i,m} + \frac{(\lambda+\beta)(D^i)^T Y^{m+1}}{\gamma\lambda\beta}, \frac{(\lambda+\beta)}{\gamma\lambda\beta}\right)$
8. ***end (while)***
9. $C^{i+1} = Y^{m+1}, \Gamma^{i+1,0} = \Gamma^{i,m+1}, D^{i+1} = D^i + \varepsilon C^{i+1}(\Gamma^{i+1,0})^T, d_q^{i+1} = \frac{d_q^{i+1}}{\| d_q^{i+1} \|_2}$, q = 1,…,Q
10. update u^{k+1} by frequency interpolation using equations 8 and 9.
11. i ← i +1
12. $f^{k+1} = f^k + f - F_p u^{k+1}$
13. $\{\hat{D}, \hat{\alpha}_{ij}, \hat{X}\} = \arg\min_{D,\alpha_{ij},X} \lambda \| X - Y \|_2^2 + \sum_{ij} \mu_{ij} \| \alpha_{ij} \|_0 + \sum_{ij} \| D\alpha_{ij} - R_{ij}X \|_2^2$ (10)
14. ***end (while)***
15. ***end (while)***

Output: A noise-free reconstructed image

---

3. Experiments and results

This section explains how the parameters used in this study were selected, data sources used in the experiments, the experimental results, and comparison with other states of art algorithms.

3.1 Parameter Selection

In our study, the parameters for the image reconstruction step were chosen based on the original implementation settings of the TBMDU algorithm [7]. The patch size $\sqrt{M}$ x $\sqrt{M}$ = 8^2, the over completeness of the dictionary K=4, and the patch overlap r=1 (corresponding Q =256 and w=$(\sqrt{M}/r)^2$ =64). Also, the parameters for the image denoising step were chosen based on the original settings by [20]. All the experiments in this paper have done using Matlab 2017a on a laptop equipped with Windows 10, Intel Core i3, 2.0GHZ CPU and 8GB RAM.

3.2 Computational cost

The number of computations in an algorithm represents the algorithm complexity and affects the run time of the algorithm. Our proposed algorithm is comprised of the TBMDU algorithm for image construction and the image denoising algorithm uses OMP for sparse coding and SimCO for dictionary learning and updating. The total computational cost for the TBMDU algorithm is $O(QMLm_{max}k_{max}P)$ where M denotes the patch size, L denotes the number of image patches and Q denotes the number of atoms. m_{max}, k_{max}, and P denote the numbers of iterations. For more details, readers can refer to Ref. [7]. For our denoising algorithm, the computational cost of OMP is $O(mnkN)$, where m is the length of the measurement vector, n is the number of atoms in the dictionary, k is the number of non-zero elements in x (sparsity) and N is the total number of patches. For dictionary learning and

updating, SimCO was used. The key characteristic of SimCO is to update all the atoms and corresponding non-zero coefficients simultaneously and hence reduce the computation cost.

The complexity of MOD and SimCO is of the same level, however the computational expense for each MOD iteration is less than that for each SimCO iteration, yet the number of iterations required for convergence in MOD is larger than that in SimCO. As opposed to MOD and SimCO where all codewords are simultaneously updated, K-SVD updates codewords individually. The overall speed of K-SVD is often slower than MOD and SimCO because of the individual update. For more details, readers can refer to Ref. [20]. Therefore, our proposed algorithm is computationally expensive because it is comprised of the individual complexities of the TBMDU algorithm, OMP, and SimCO. When compared to TBMDU and DLMRI algorithms, the computational cost of the DLMRI algorithm is *O(nKTN)*, where n is the size of the patches, K represents the number of atoms, T is the sparsity threshold for each patch and N is the total number of patches. The computational cost of the DLMRI is higher than that of the TBMDU algorithm, because the dictionary update of K-SVD uses the complicated SVD decomposition, while TBMDU method only involves simple matrix multiplication. For more details, we refer the reader to Ref. [8]. Therefore, our proposed algorithm is computationally more expensive when compared to TBMDU and DLMRI algorithms but it is more noise-robust when compared to the two algorithms.

3.3 Data Sources

The image data used during this study was obtained from the low-field MRI systems that are currently at Pennsylvania State University (PSU) and Leiden University Medical Centre (LUMC). Both systems are still in development and the images used are available on request. Also, a real MRI image was used during the experiment. The image was obtained from [8].

3.4 The Performance Metrics Used

During this study, we adopted the performance metric that were used by other researchers in related studies. The metric is Peak Signal to Noise Ratio (PSNR) [8] [17]. PSNR (measured in decibels-dB) is computed as the ratio of the peak intensity value of the reference image to the root mean square (RMS) reconstruction error relative to the reference image. This metric is considered as the image quality measure and has been used a lot in image compression and denoising tasks. However, PSNR does not represent perceptual visual quality, which can be assessed by a human observer.

3.5 Results

The phantom image in Figure 1.2 was used in our experiments during this study. We also tested our algorithm on an image used in [8]. We compared the performance of our algorithm with TBMDU and DLMRI using the PSNR metric and the execution time.

(a) Comparative Performance of the algorithms basing on PSNR, the Execution Time (s) and the CPU_time

(i) Using a Phantom Image

The PSNR, the Execution Time (s) and the CPU_time were recorded after 20 iterations using a phantom image in Figure 1.2 (middle), as shown in Table 1 below. It can be noted that our proposed algorithm has a higher PSNR when compared to the TBMDU and DLMRI algorithms. However, our proposed algorithm has a higher execution time and CPU time when compared to the TBMDU and DLMRI algorithms.

Table 1: Performance of the algorithms using a Phantom Image

Parameter	TBMDU	DLMRI	Proposed Algorithm
PSNR (dB)	30.2	30	33.8
Execution Time (s)	149.5871	380.8340	631.0341
CPU_time	3.9013e+03	4.1301 e+03	4.4460e+03

(ii) Using MR image from [8]

The PSNR, the Execution Time (s) and the CPU_time were recorded after 20 iterations using the MR image from [8], as shown in Table 2 below. It can also be noted that our proposed algorithm has a higher PSNR when compared to TBMDU and DLMRI algorithms. Our proposed algorithm also has a higher execution time when compared to TBMDU and DLMRI algorithms. Also, our proposed algorithm have a low CPU time when compared to TBMDU and DLMRI algorithms.

Table 2: Performance parameter of the algorithm

Parameter	TBMDU	DLMRI	Proposed Algorithm
PSNR (dB)	38.2	38.3	38.5
Execution Time (s)	148.0857	370.9409	617.2350
CPU_time	3.6761e+03	3.8257e+03	3.4443e+03

(iii) Using MR image from [8]after adding 20dB of noise

The PSNR, the Execution Time (s) and the CPU_time were recorded after 20 iterations using the MR image from [8], as shown in Table 3 below. It can be noted that our proposed algorithm has a higher PSNR when compared to DLMRI algorithm, and approximately the same value when compared to TBMDU. Our proposed algorithm also has a higher execution time and CPU time when compared to TBMDU and low execution time when compared to DLMRI.

Table 3: Performance parameter of the algorithm

Parameter	TBMDU	DLMRI	Proposed Algorithm
PSNR (dB)	2.951014e+01	2.874695e+01	2.945824e+01
Execution Time (s)	235.8519	1.4944e+03	299.7162
CPU_time	7.8357e+03	7.1346e+03	9.3852e+03

(b) Image Reconstruction using our proposed algorithm, DLMRI and TBMDU

(i) Using a Phantom Image

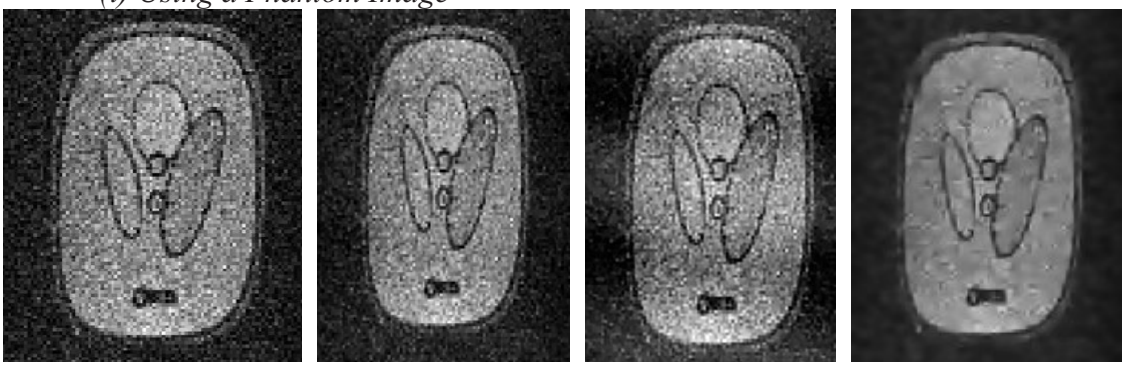

(a) **(b)** **(c)** **(d)**

Figure 1.3: The original image (a) that was used for reconstruction. The results after 10 iterations for TBMDU, DLMRI and our proposed algorithm were (b), (c) and (d) respectively.

After 20 iterations, a phantom in Figure 1.3 was reconstructed using TBMDU, DLMRI and our proposed algorithm. The results are shown in Figure 1.3. It can be

noted that our proposed algorithm is robust to noise when compared to TBMDU and DLMRI algorithms.

(ii) Using the MR image from [8]

After 20 iterations, a real MRI image was reconstructed using TBMDU, DLMRI and our proposed algorithm. The results are shown in Figure 1.4. It can be noted that our proposed algorithm also performs better when compared to TBMDU and DLMRI algorithms.

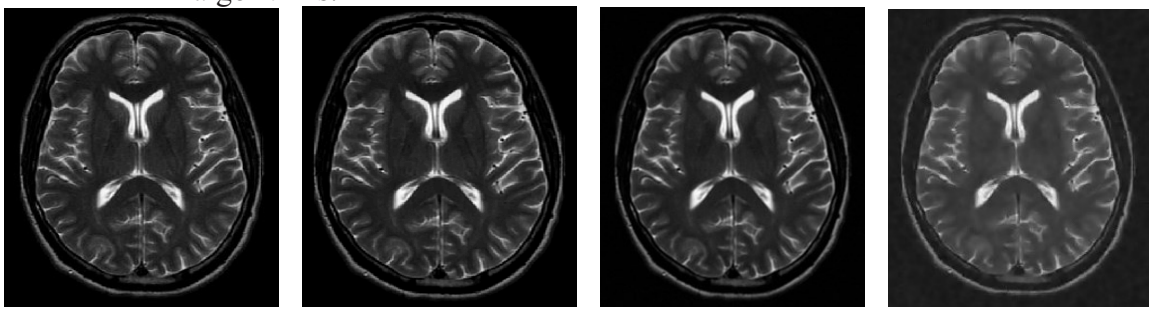

(a) (b) (c) (d)

Figure 1.4: The original MRI image (a). The results after 10 iterations for TBMDU, DLMRI and our proposed algorithm were (b), (c) and (d) respectively.

(iii) Using MR image from [8]after adding 20dB of noise

During this experiment, we used again the MR image from [8] (a). This image was corrupted by 20dB of noise and was used to train the dictionary (b). We were then interested to reconstruct the image corrupted by noise. After 20 iterations, the image was reconstructed using TBMDU, DLMRI and our proposed algorithm. The results are shown in Figure 1.5. Visually, it was noted that our proposed algorithm performed relatively better when compared to TBMDU and DLMRI algorithms.

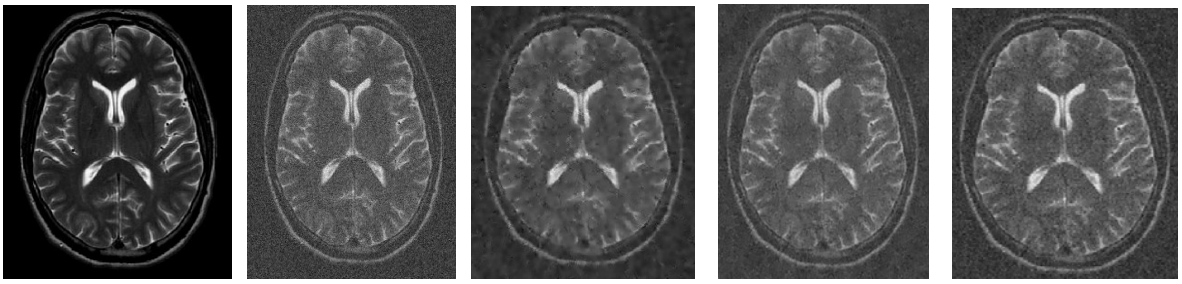

(a) (b) (c) (d) (e)

Figure 1.5: (a) is the original image, (b) we added 20dB of noise to the original image, (c) a reconstruction of b using our proposed algorithm, (d) reconstruction of b using DLMRI and (f) is the reconstruction of b using TBMDU

4. Discussion

The results of this study were compared with the TBMDU and DLMRI algorithms. The later algorithm (DLMRI) has been used as a benchmark algorithm in studies related to image reconstructions in MRI using Compressed Sensing (dictionary learning) techniques. TBMDU was also used for comparison because it outperformed DLMRI, a technique that substantially outperformed other CSMRI based reconstruction methods (For more details we refer the readers to Ref. [7]). By visual inspection (see Figures. 1.3, 1.4 and 1.5), it was observed that our proposed formulation outperforms the TBMDU and DLMRI algorithms especially when the input image to be reconstructed is corrupted with noise. However, it was noted in all our experiments that the TBMDU algorithm converges faster, followed by DLMRI and lastly, our proposed algorithm. The proposed algorithm was not compared with

Deep learning techniques due to the computational complexity of Deep Learning algorithms, e.g. the need for graphical processing units (GPUs) during training, and also large training datasets are required for deep learning algorithms to perform well. During this study, only one image was required for dictionary training per experiment and also no additional computing power like GPUs was required during our experiments which in contrast is required for Deep Learning experiments. Therefore, this algorithm is practically applicable to the low-field MRI systems. These systems are characterized by low signal to noise ratio and therefore the final images have noise which needs to be removed before the image is used for clinical use. The algorithm developed during this study is important for the final MRI product because of its robustness to noise. The results of the study demonstrated that the algorithm is effective in removing noise during the reconstruction process.

5. Conclusions and Outlook

The paper discussed a compressed sensing-based image reconstruction algorithm that combines both reconstruction and denoising. Authors of this paper were motivated by the fact that noise is inseparable from imaging modalities and therefore having an algorithm that jointly reconstructs and denoises an image or a signal could save time other than working on two operations differently. Results from the experiments demonstrated that our proposed algorithm performed well especially when the input image to be reconstructed is noisy. Image denoising is an important procedure required before image analysis tasks like segmentation, classification and also in computer vision tasks; therefore our proposed algorithm is suitable for performing noise-robust reconstructions which is essential for image analysis tasks. Combining the two could save time and other image details that could be lost due to having two separate operations. This formulation is essential in imaging modalities like low-field MRI where the image signal is noisy and therefore performing a joint reconstruction and denoising could help improve the quality of the images obtained.
The next step in our research is to combine our algorithm with the low-field hardware and image processing software that has been developed within our project [2,4,5] and to thesis of Venkateswararao Cherukuri [21] for further evaluation and testing. To this end we are currently replicating the MRI devices at MUST and unifying our software. We expect to be ready for medical trials which will be performed jointly with CURE children hospital Uganda in 2021.

Acknowledgment

This research was made possible through the Dutch organization NWO-WOTRO grant nr. W 07.303.101:‘A sustainable MRI system to diagnose hydrocephalus in Uganda’. The authors gratefully acknowledge NWO for their financial support. We also thank the referees for their comments which helped us to improve this paper, S. Ravishankar for making the DLMRI code and an MRI image publically available, Qiegen Liu for making the TBMDU code publicly available, Wei Dai for making the SimCo code publically available and finally Merel Lisanne De Leeuw Den Bouter and Dilan Burçin Gecmen from TU Delft, for the wonderful discussions.

Conflict of Interests

This paper has the assent of all co-authors and the authors declare that there are no conflicts of interest regarding the publication of this paper.

References

[1] C. Guo, “Machine Learning Methods for Magnetic Resonance Imaging Analysis,” The University of

Michigan, 2012.
[2] J. Obungoloch *et al.*, “Design of a sustainable prepolarizing magnetic resonance imaging system for infant hydrocephalus,” *Magn. Reson. Mater. Physics, Biol. Med.*, pp. 1–21, 2018, doi: 10.1007/s10334-018-0683-y.
[3] M. de L. den Bouter, “Image reconstruction in low-field MRI : A super-resolution approach,” Delft University of Technology, 2017.
[4] T. O. Reilly and A. Webb, “Deconstructing and reconstructing MRI hardware,” *J. Magn. Reson.*, vol. 306, pp. 134–138, 2019.
[5] M. L. de L. den Bouter, M. B. van Gijzen, and R. F. Remis, “CGME for general-form regularization with an application to low-field MRI,” 2018.
[6] D. L. Donoho, “Compressed Sensing,” *IEEE Trans. Inf. Theory*, vol. 52, no. 4, pp. 1289–1306, 2006.
[7] Q. Liu, S. Wang, K. Yang, J. Luo, Y. Zhu, and D. Liang, “Highly Undersampled Magnetic Resonance Image Reconstruction Using Two-Level Bregman Method With Dictionary Updating,” *IEEE Trans. Med. Imaging*, vol. 32, no. 7, pp. 1290–1301, 2013.
[8] S. Ravishankar and Y. Bresler, “MR Image Reconstruction From Highly Undersampled k-Space Data by Dictionary Learning,” *IEEE Trans. Med. Imaging*, vol. 30, no. 5, pp. 1028–1041, 2011.
[9] E. Plenge, M. A. Cooper, M. R. Prince, Y. Wang, P. Spincemaille, and M. Elad, “Reconstruction of Highly Under-Sampled Dynamic MRI using Sparce Representation of 1D Temporal Snippets,” *978-1-4799-2374-8/15/2015 IEEE*, pp. 1240–1243, 2015.
[10] Y. Cong, S. Zhang, and Y. Lian, “K-SVD Dictionary Learning and Image Reconstruction Based on Variance of Image Patches,” in *Proceedings - 2015 8th International Symposium on Computational Intelligence and Design, ISCID 2015*, 2016, vol. 2, no. 3, pp. 254–257, doi: 10.1109/ISCID.2015.148.
[11] J. Liu, S. Wang, X. Peng, and D. Liang, “Undersampled MR Image Reconstruction with Data-Driven Tight Frame,” *Comput. Math. Methods Med.*, 2015.
[12] J. Li, Y. Song, and J. Zhao, “Dual-Dictionary Learning Based MR Image Reconstruction with Self-adaptive Dictionaries,” *978-1-4244-9270-1/15/2015 IEEE*, no. 1, pp. 7051–7054, 2015.
[13] A. Majumdar and R. K. Ward, “Compressed Sensing Based MR Image Reconstruction from Multiple Partial K-Space Scans,” *978-1-4577-1921-9/11/2011 IEEE*, no. 3, pp. 340–343, 2011.
[14] T. Tong, J. Caballero, K. Bhatia, and D. Rueckert, “Dictionary learning for medical image denoising, reconstruction, and segmentation,” in *Machine Learning and Medical Imaging*, no. Dl, Elsevier Inc., 2016, pp. 153–181.
[15] M. Elad and M. Aharon, “Image Denoising Via Learned Dictionaries and Sparse representation,” in *2006 IEEE Computer Society Conference on Computer Vision and Pattern Recognition (CVPR’06)*, 2006, doi: 10.1109/CVPR.2006.142.
[16] S. Cai, Z. Kang, M. Yang, X. Xiong, and C. Peng, “Image Denoising via Improved Dictionary Learning with Global Structure and Local Similarity Preservations,” *MDPI-Symmetry*, pp. 1–20, 2018, doi: 10.3390/sym10050167.
[17] M. Elad and M. Aharon, “Image Denoising Via Sparse and Redundant Representations Over Learned Dictionaries,” *IEEE Trans. Image Process.*, vol. 15, no. 12, pp. 3736–3745, 2006.
[18] Y. C. Pati, R. Rezaiifar, and P. S. Krishnaprasad, “Orthogonal Matching Pursuit : Recursive Function Approximation with Applications to Wavelet Decomposition,” in *To appear in Proc. ofthe 27 Annual Asilomar Conference on Signals Systems and Computers, Nov. 1-3, 1993*, 1993, pp. 1–5.
[19] M. Aharon, M. Elad, and A. Bruckstein, “K -SVD : An Algorithm for Designing Overcomplete Dictionaries for Sparse Representation,” *IEEE Trans. Signal Process.*, vol. 54, no. 11, pp. 4311–4322, 2006.
[20] W. Dai, T. Xu, and W. Wang, “Simultaneous Codeword Optimization (SimCO) for Dictionary Update and Learning,” *IEEE Trans. Signal Process.*, vol. 60, no. 12, pp. 6340–6353, 2012.
[21] V. Cherukuri, P. Ssenyonga, B. C. Warf, A. V. Kulkarni, V. Monga, and S. J. Schiff, “Learning based segmentation of CT brain images: Application to postoperative hydrocephalic scans,” *IEEE Trans. Biomed. Eng.*, vol. 65, no. 8, pp. 1871–1884, 2018, doi: 10.1109/TBME.2017.2783305.